HWOT-scaled Cascade fractional order hybrid controller applied to Renewable based EV generating systems

Basudeb Mondal, Soumen Biswas, Provas Kumar Roy and Susanta Dutta

Basudeb Mondal is with Electrical Engineering Department,
Dr B.C. Roy Engineering College, Durgapur, India, e-mail:basudeb.705@gmal.com
Soumen Biswas is with Electrical Engineering Department,
Dr B.C. Roy Engineering College, Durgapur, India, e-mail: soumeniitkgp10@gmail.com
Provas Kumar Roy is with Electrical Engineering Department,
Kalyani Government Engineering College, India, e-mail: roy_provas@yahoo.com.
Susanta Dutta is with Electrical Engineering Department,
Dr B.C. Roy Engineering College, Durgapur, India, e-mail:susanta.dutta@bcrec.ac.in

December 21, 2022

ABSTRACT

In the upcoming epochs, conventional energy may deplete soon. Thus, the use of conventional energy in the power industries need to be supplemented by non-conventional energy resources. This would result in loss of synchronisms in the power grids owing to the fact that solar and wind alternate their attributes expeditiously with change in atmospheric phenomenon. To ameliorate frequency deviation within a specific range automatic generation control (AGC) implements forced allowance on system operation. A three area thermal with photovoltaic (PV), electric vehicle (EV), wind system is considered under deregulated environment to develop and to judge the efficacy of newly developed cascade fractional order hybrid controller combination of (FOTID & 3DOF-PID). Comparing the aforementioned controller to other controllers such as the three degree of freedom proportional-integral-derivative (3DOF-PID), the fractional order tilt-integral-derivative (FOTID), and the proportional-integral-derivative (PID) justifies the system's effectiveness. This assessment has been accomplished by a trendy optimization technique such as hybrid whale optimization algorithm (HWOT). However, the main intent of this write-up is to fabricate a cascade fractional order (CC-FO) hybrid controller that would act as the new control mechanism for the proposed system under deregulated scenario. It has been found that the suggested CC-FO hybrid controller stabilises the system (*i.e.*, Under step load disruptions, frequency deviation and tie-line power become zero) in the shortest amount of time possible. Additionally, it is seen that the recommended controller can control a wide range of nominal loading circumstances and system characteristics, demonstrating its robustness.

Keywords:
Automatic generation control (AGC); Renewable sources (Solar, EV & Wind) ; EV (Electric Vehicle), Photovoltaic (PV), Deregulated system; Hybrid whale optimization algorithm (HWOT); CC-FO Hybrid controller (FOTID & 3DOF-PID); Fractional Order Tilt-Integral–Derivative (FOTID)

1. Introduction

A power system is said to be a dependable power system if it is always capable of maintaining a continuous balance betwixt the quantity of power generated at the power station and the load availability. In order to preserve equilibrium, the system frequency must be kept at a specific level. Automatic generation control (AGC) is essential for preserving the system's

transients and harmonics as well as the tie power at the optimum level. Basically, AGC acts as a connecting link between the dispatch centre and its corresponding generating station. AGC is employed to control and regulate the generator output to obtain the desired system parameters. To keep a note on the changes in power system government proposed some new set of rules by involving the private participants and enlarging customer involvement in the electricity. This process is known as deregulation.

In this article a multi source system consisting of both renewable and non-renewable is considered under deregulated environment and it made to meet the varying load demand under peak load condition. In the deregulated market, the conventional vertically integrated utility (VIU) is restructured into horizontal integrated utility (HIU) consisting of different bodies, viz. generation company (GENCOs), transmission companies (TRANSCOs) and distribution companies (DISCOs).[1] Following investigations on the AGC controllers and algorithms employed by different multi-source power networks in a deregulated environment, we discovered that the majority of researchers are focusing on AGC in multi-source power systems using different types of PID and TID controllers tuned with various optimization techniques like whale optimization (WO), water wave optimisation (WWO), dragonfly search algorithm and so on. Keeping this objective in mind, we have proposed a FOTID controller tuned using hybrid whale optimization algorithm (HWOT) to have a detailed study in the given field of AGC.
Below is a list of several researchers' analyses. A hybrid teaching learning based optimization and pattern search (hTLBO-PS), tilted integral derivative (TID) controller has been proposed for AGC in a deregulated environment [2]. They assumed a two-area four units thermal-gas system to analyze the superiority of the proposed controller and finally sensitivity analysis of the suggested methods was carried out with perturbation in plant parameters. Pathfinder algorithm (PFA) tuned FOTID controller is another metaheuristic optimization technique as proposed by [3] for AGC of multi-source power system. To demonstrate the effectiveness of the proposed controller under erratic load variations, they performed simulation studies on an interconnected two-area power system made up of different sources, including thermal, hydro, and gas generating units.They also included physical constraints, such as governor dead band (GDB), and generation rate constraint (GRC). Soni *et al*. [4] and team mates proposed another meta-heuristic approach called as "grey wolf optimization" tuned 2DOFPID controller for AGC of multiarea interconnected power systems and proved that better dynamic response with less number of oscillations and overshoots are observed in the system using the proposed technique. Sahu *et al*. [5] along with his team implemented differential evolution (DE) algorithm on TID with filter (TIDF) for AGC of a multi area reheat thermal power system considering the physical parameters such as generation rate constraint and governor dead band non linearity. In the year 2019 an alternative controller called as the optimized fuzzy FOPI-FOPD controller optimized using the imperialist competitive algorithm (ICA) was proposed by Arya *et al*. [6] to deal with the AGC of isolated and interconnected multi-area power systems. The designed system was put to the test by being compared to different alternative control methods in terms of least error and metrics like undershoots, overshoots, and settling duration of frequency and tie-line power deviations relating to an abrupt load demand in a specific location. A similar study was presented by RanjanNayak *et al*. [7] and team wherein a comparison of type-2 fuzzy-PID controller performance is shown using the adaptive-SOS algorithm (ASOS) for AGC of a networked power system. In order to illustrate the superiority of the proposed ASOS algorithm over SOS algorithm, they have conducted a thorough examination of the transient performance of the AGC system by applying a sudden step load shift of 10% in area-1 of the two unequal area power system. Another paper was published by RanjanNayak *et al*. in the year 2021 [8] wherein for the AGC of small hydro plants integrated multi-area system, a fuzzy based symbiotic organism search optimised hybrid PID fuzzy-PID controller was developed. They solved nine benchmark equations to show how the suggested controller functions. Using enhanced responses from second, third, and fourth order systems, the effectiveness of the suggested controller was determined. Further, a similar research was carried out by Rajesh *et al*. [9] which was based on the frequency control of five area power systems using hybridised firefly optimization algorithm and Pattern Search technique (hIFA-PS) aided PID controller to tune the parameters of fuzzy . By taking into account various controller architectures and doing a comparison study of hIFA-PS optimised I/PI/PID/Fuzzy aided PID, the dynamic performance of the controllers was enhanced. Simhadri *et al*[10] suggested a whale optimization algorithm (WOA) that improved a two-degree-of-freedom tilt integral derivative with filter (2DOF TIDF) controller to control AGC issues in a two-area hydro-thermal system. Elephant herding optimization(EHO) was used for AGC of Interconnected Power Systems is studied in variations of load demands by using MATLAB/Simulink for uncertain Dhillon *et al*. [11]. Irudayaraj *et al*. [12] proposed a Matignon's theorem based atom search optimized FOPID Controller for load frequency control of HFS. They tested the proposed controller on a two-area HPS that was created with the aid of MATLAB/Simulink and later compared to similar literature works in order to ensure its robustness. A similar study was conducted by Shouran *et al*. [13] where he and his team developed a Fuzzy PIDF, FOPID controller whose parameter was tuned using the bees algorithm (BA) for LFC of the great britain (GB) power system. They tried proving robustness of the proposed system in balancing that frequency of the great Britain power system by comparing their controller with controllers which were tuned using the particle swarm optimization (PSO) algorithm and Teaching learning-based optimization (TLBO) and used it for the same considered systems. Kumar *et al*. [14] designed a robust PIDD2 Controller for preturbed Load frequency control of Interconnected time-delayed power systems. They tuned the PIDD2 controller using internal model control (IMC) algorithm. The controller efficiency was verified by assessing the system considering its corresponding parametric uncertainties as well as

in the CTD, non-linearities, and step load disturbances and the delay margin was calculated with the aid of Walton and Marshall stability theorems. Similarly, Bagheri *et al.* [15] designed a ABC-based terminal sliding mode controller optimized using artificial bee colony (ABC) optimization algorithm for balancing the frequency of the load of an islanded micro-grids system at a rated value. Tribe-DE optimization algorithm-tuned fuzzy self-tuning PID controller was proposed by Jalali *et al.* [16] for controlling the frequency of the load of interconnected multi-area power systems. They examined the proposed strategy on power systems in the two and three area interconnected subject to various conditions and assuming the Integral Time Absolute Error (ITAE) less than 0.0108 furthermore keeping the regulation's absolute maximum undershoot below 0.0210 Hz. Sobhy *et al.* [17] with his team used Marine predators algorithm for optimizing PID controllers to adjust the load frequency of the connected power networks of the current era more quickly and effectively which comprises of renewable energy sources and energy storage units. They involved three types of RESs in their literature which includes wind, photovoltaic and thermal. Superconducting magnetic energy storage (SMES) and battery energy storage (BES) were included in the supposed system, and real data were imported into the RESs to demonstrate the effectiveness of the suggested system. In parallel a proportional integral–fractional order proportional derivative (FOPI–FOPD) cascade controller optimised using dragonfly search algorithm was developed by Çelik *et al.* [18] for high-performance thermal PS control methods with/without GDB non-linearity for two-area thermal. The major goal of the experiment was to reduce the frequency and tie-line power variations' integral time absolute error (ITAE). The robustness of the system was explained by comparing it with other similar controllers. A correlative study was performed by Guha *et al.* [19] on cascade fractional-order 3DOF-PID controller optimised using equilibrium optimizer (EO) with an aim of addressing the issue of load frequency regulation in a connected power system that incorporates a DFIG-driven wind power system. Further studies were conducted by Yousri *et al.* [20] wherein he implemented Proportional–Integral (PI) controller optimised using Harris hawk optimizer for achieving better load frequency control operation of multi-interconnected renewable energy plants. Mishra *et al.* [21] proposed and implemented a method for LFC of AC multi micro-grid (MG). The methods involves the use of hybrid FOFPID controller and linear quadratic Gaussian (LQG), the controller being optimised using multi-verse optimization (MVO) algorithm. They justified the efficacy of the proposed algorithm by comparing with Particle Swarm and genetic algorithm. *et al.* Khokhar [22] implemented fractional order proportional integral derivative plus second-order derivative (FOPID+DD) optimised using water wave optimisation (WWO) algorithm for the LFC of a hybrid power system (hPS) incorporating conventional and certain distributed generation sources.Multiple disturbances and non-linearities, such as generation rate constraints, governor dead bands, and temporal delays connected to the hPS, were taken into account in order to demonstrate the superiority and effectiveness of the suggested controller. Similarly, Kumar *et al.* [23] To address the different issues experienced during its load frequency control, a two-area deregulated hydro-thermal power system installed a whale optimization (WO) controller. Many more similar studies was carried out by various other researchers like : Amiri *et al.* [24] implemented FOPID controller tuned by hybrid craziness-based particle swarm optimization (CRPSO) and pattern search (PS) in isolated microgrid; Ram Babu *et al.* [25] Coyote optimization algorithm was used to implement PI minus DF Controller in Multi-area System Including Dish-Stirling Solar Thermal System (COA); Sahin *et al.* [26] implemented Fractional High Order Differential Feedback Controller optimised using particle swarm optimization (PSO) algorithm in multi-area power systems ; Khokhar *et al.* [22] proposed hybrid Fuzzy PD-TID Controller tuned by chaotic crow search algorithm (CCSA) in a Standalone Microgrid ;Shakibjoo *et al.* [27] proposed type-2 fuzzy inference systems (IT2FIS) and fractional-order controller optimised using Levenberg–Marquardt algorithm (LMA) implemented in multi-area power systems. All aimed at controlling load frequency at the rated value of various realistic systems in a more efficient way. In light of the foregoing discussion, the noble aims of the paper are summarized below:

i) A new controller named the Cascade fractional order hybrid controller (CCFOHC) tuned with hybrid whale optimization algorithm is devised and implemented on the aforementioned system to solve the problem of the renewable energy-based system.

ii) Expand the analysis to a three-area system that includes solar, wind, and EVs (electric vehicles) in a deregulated environment.

iii) The performance of the proposed controller is then contrasted with that of a number of existing controllers, including 3DOF-PID, FOTID (fractional-order tilt-integral-derivative), and the TID controller alone.

iv) By exposing the produced controller to a wide range of nominal loading situations as well as system characteristics, the resilience of the developed controller and the optimization process is demonstrated. $\pm 0.2.u(Mw)$.

2. Static model and mathematical analysis description

In this literature how effective the suggested CC-FO-hybrid (cascade fractional order hybrid) Controller is compared to traditional controllers in a three-area deregulated system is taken into consideration to keep the schedule frequency level in the electricity industry's competitive environment. Here, a doubly-fed induction generator (DFIG) driven wind power system (WPS) integrated model with a three-area interconnected non-reheat thermal power system has been studied. The power system itself, the steam turbine, and the speed governor are all included in each control area. A WPS model incorporates the two-mass model of the mechanical connection shaft, wind aerodynamics, and DFIG. Whereas in the other part, solar

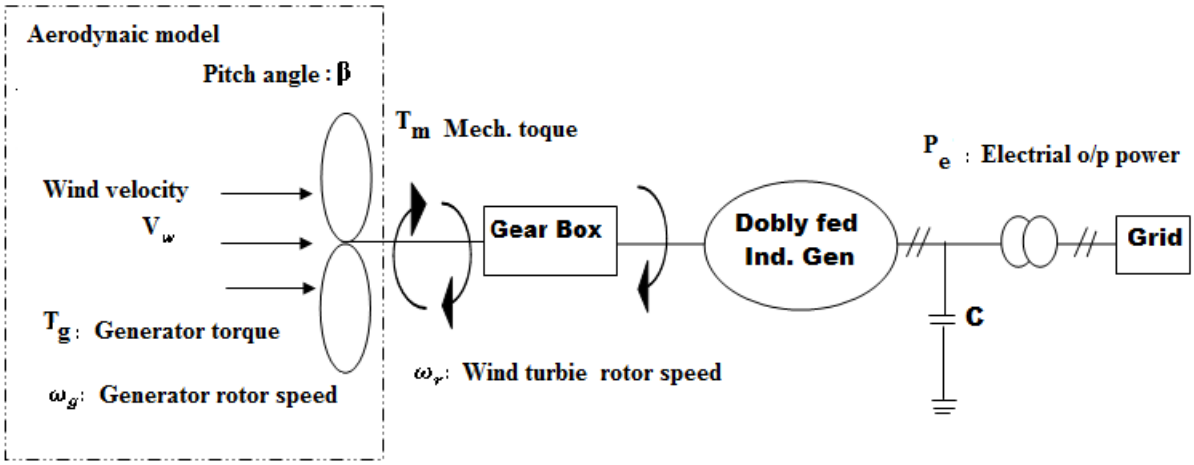

Figure 1: Schematic diagram of Wind Turbine

(PV system) is combined with thermal units, along with conventional thermal units and EV (Electric Vehicle system) also incorporate to a thermal unit.

In order to test the effectiveness of the suggested controller with the suggested HWOT (hybrid whale optimization) algorithm in a realistic setting, several nonlinear constraints, such as governor dead-band (GDB), boiler dynamics (BD), and generation rate constraints (GRC), are added to the proposed system.

2.1 Modeling of wind power system

Variation in frequency and interchange in tie-line power due to irregular intervals of output in WPS, experiences in the conventional power system. The wind aerodynamic model, mechanical coupling shaft, and DFIG are taken under this model of WPS comprises. In the following subsections all components are explained which are including in the model of WPS.

2.1.1 Wind aerodynamic model

In a Wind turbine generated system,wind turbine rotor speed (ω_r) and mechanical torque (T_m) which are coupling between them shown in Fig. 1 provides in the aerodynamic model. According to the variation of time, wind speed and atmospheric pressure fluctuates the output power of WPS. The WPS is proportional to the cube of upstream wind speed (V_ω), from where mechanical power (P_{mech}) derived. A certain amount of wind energy extracts by the wind turbine from the wind, expressed by the rotor power coefficient (C_r). The theoretical upper limit is maximum than the rotor power coefficient's maximum value C_r^{max}.

The wind power available, the machine's power curve, and the machine's capacity to adapt to wind fluctuation all play a role in how much power a wind turbine can extract. The formula for wind-generated power is given by:

$$P_{mech}(V_\omega) = \frac{1}{2} C_r(\gamma, \delta) \rho \Pi R^2 V_\omega^3 \tag{1}$$

Where ρ is air density, R is radius of rotor, V_ω is wind speed, C_r denotes rotor power coefficient of wind turbine,γ is the tip-speed ratio and δ represents pitch angle. Note that the tip-speed ratio is defined as:

$$\gamma = \frac{R\omega_r}{V_\omega} \tag{2}$$

If the rotor speed is maintained, it is observed that any change in wind speed would alter the tip-speed ratio, which will alter the rotor power coefficient γ_q as well as the power produced by the wind turbine. However, if the rotor speed is modified in accordance with the variation in wind speed, the tip-speed ratio can be kept at a desirable level, which could result in the system's maximum power output.

From eqs.(1) and (2) we calculate

$$P_{mech}(\omega_r) = K_w \omega_r^3 \tag{3}$$

Where,

$K_w = \frac{1}{2} C_r \rho \Pi \frac{R^5}{\gamma^3}$

The main work concept is shown in the simplified block diagram that follows Fig. 1 for a typical wind power generation system. We can see that the main components of such a system are an aero turbine, which transforms wind energy into mechanical energy, a gearbox, which increases speed and reduces torque, and a generator, which transforms mechanical energy into electrical energy.

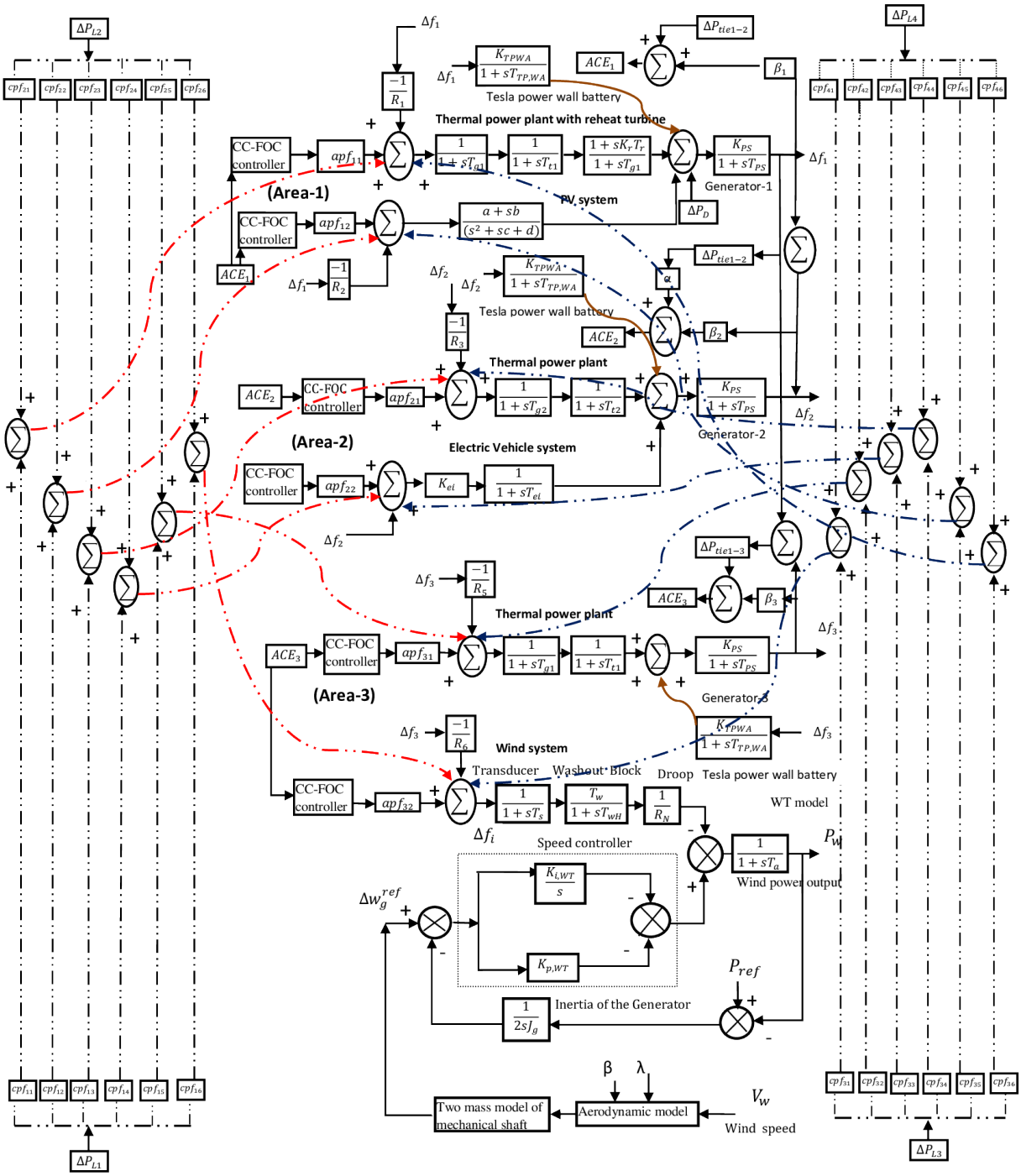

Figure 2: Linearized model diagram of three area thermal with solar(PV), Electric vehicle (EV), wind system.

2.1.2 Mechanical coupling shaft

The wind turbines rotor rotates at a speed of (ω_r) while being propelled by the input wind torque (τ_m). The generator then receives the transmission output torque (τ_p), producing a shaft torque of (τ_s) at generator angular velocity of (ω_a).

Due to the employment of the gearbox, it should be noted that the rotor speed and generator speed are generally not the same.

Output of the aerodynamic model (the mechanical torque) is transferred through a mechanical coupling shaft to an asynchronous generator's rotor. In Fig. 1 by a two-mass model, this mechanical shaft can be represented and also a high-speed generator through a gear-box is coupled with a low-speed wind turbine. The flexible shaft connecting the high-speed generator and low-speed turbine is secured by a spring and a damper. The following equations can be used to describe the system's dynamics:

$$\tau_m - \tau = J_m\dot{\omega} + B_m\omega_s + K_m\theta \tag{4}$$

$$\tau_p - \tau_e = J_e\dot{\omega_e}B_e\omega_e + K_e\theta_e \tag{5}$$

$$\tau_p\omega_e = \tau_m\omega_s \tag{6}$$

where B_m,K_m, B_e, K_e are the friction- and torsion-related constants τ_m, τ_e, τ, τ_p the shaft torque seen at turbine end, generator end, before and after gear box, J_m, J_e the moment of inertia of the turbine and the generator, (ω_s) and (ω_e), the angular velocity of the shaft at turbine end and generator end.

Model of the mechanical shaft express by the differential equation(5 and 6) is given by

$$\omega_r = -\left(\frac{D_r + D_{sh}}{J_w}\right)\omega_r + \left(\frac{D_{sh}}{J_w}\right)\omega_g - \left(\frac{1}{J_w}\right)T_{int} + \left(\frac{1}{J_w}\right)T_m \tag{7}$$

and

$$\omega_g = -\left(\frac{D_g + D_{sh}}{J_g}\right)\omega_g + \left(\frac{D_{sh}}{2J_g}\right)\omega_r - \left(\frac{1}{J_{ge}}\right)T_g + \left(\frac{1}{G_n J_g}\right)T_{int} \tag{8}$$

T_m mechanical torque.
D_{sh} damping coefficients of coupling shaft.
A_g air-gap torque of the induction generator.
J_w inertia parameters of wind turbine.
J_g inertia parameters of generator.
D_r rotor's damping coefficients of wind turbine's.
D_g rotor damping coefficients of generator.
T_{int} internal torque of the model.
G_n gear train ratio.

2.1.3 Electric Vehicle

Typically, Electric Vehicle unit serves as the production of electrical energy in a stand-by power station. This power plant serves as an additional source of power that may be placed wherever it is needed. Limited quantities of electrical energy can be produced at this type of power plant, which can serve as emergency supply hubs.

2.1.4 Battery source

In order to ensure a consistent power flow over a tie-line during intermittent load demand, particularly during the peak demand period, storage renewable energy resources are used. The following explains the function of battery energy storage devices in the grid, including super-magnetic energy storage devices, redox-flow batteries, and Tesla power wall batteries:-

- Keep the various generating units properly coordinated.
- Reduce operating costs.
- The power converter and bank of D. C. batteries make up the BESS. According to the needs of the grid, power converters are useful for bi-directional power conversion (from DC to AC and vice versa).
- It is also used to regulate the system voltage and to neutralize the harmonics in the system.

stability using the HWOT optimization technique. In addition with that, three area thermal with solar(PV), Electric Vehicle (EV), wind system is accounted to explain the design methodology of the proposed controller which is shown in Fig. 2. The nominal parameters of the given system are specified in Appendix-A. From this Fig. 2 it is clearly seen that a conventional reheat type thermal power plant jointly generates power with non-conventional wind and solar power plant in deregulated scenario.

Also, in this article the test systems are considered under deregulated condition for the restructured power market. Generation, Transmission and distribution of electric power is carried out jointly by various bodies, viz. GENCOs, TRANSCOs and DISCOs.

$$\text{DPM} = \begin{bmatrix} f_{11} & f_{12} & f_{13} & f_{14} & f_{15} & f_{16} \\ f_{21} & f_{22} & f_{23} & f_{24} & f_{25} & f_{26} \\ f_{31} & f_{32} & f_{33} & f_{34} & f_{35} & f_{36} \\ f_{41} & f_{42} & f_{43} & f_{44} & f_{45} & f_{46} \\ f_{51} & f_{52} & f_{53} & f_{54} & f_{55} & f_{56} \\ f_{61} & f_{62} & f_{63} & f_{64} & f_{65} & f_{66} \end{bmatrix} \tag{9}$$

Two types of contract work between the DISCO and GENCO. They are namely : unilateral contract(where the DISCO makes the contract with the GENCO within the same arena) and bilateral contract(where the DISCO makes the contract with the GENCO of some other area). All these possible contracts between GENCO and DISCO can be represented in a matrix form known as DISCO participation matrix (DPM) where the rows of the matrix depicts the GENCO and the columns depicts the DISCO. The coefficients reflects the fraction of load contract in DISCOs towards a GENCOs. Let us consider, two DISCOs ($DISCO_1$, $DISCO_2$) and three GENCOs ($GENCO_1$, $GENCO_2$ & $GENCO_3$). Therefore, the disco participation matrix (DPM) may be defined as follows [1] given in (9). Summation of all columns elements is unity and this may be mathematically given as:

$$\sum_{\text{n=1}}^{\text{NGENCO}} \text{f}_{\text{nm}} = 1;\text{for}\ \ \text{m} = 1,2,3 \ldots\ldots\ldots \{NDISCO\} \tag{10}$$

Where, NGENCO = total number of GENCOs
NDISCO = total number of DISCOs.

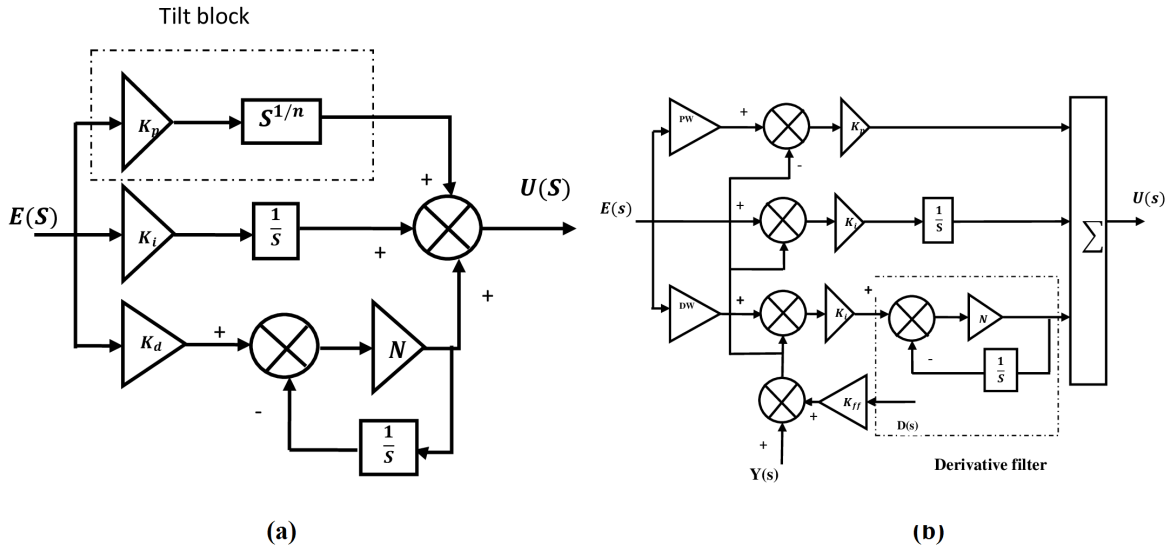

Figure 3: (a)Slave controller 3DOF-PID.(b)Master tilt integral controller

Now, the contract power schedule of n^{th} GENCO with DISCO is:

$$\Delta \mathrm{P} \sum_{\mathrm{m}=1}^{\mathrm{NDISCO}} \mathrm{CP}_{\mathrm{nm}} \Delta \mathrm{P}_{\mathrm{L}} \text{for n} = 1,2,3 \cdots \cdot \mathrm{NGENCO} \tag{11}$$

$$\sum_{\mathrm{n}=1}^{\mathrm{NGENCO}} \mathrm{f}_{\mathrm{nm}} = 1 \quad \text{for} \quad \mathrm{m} = 1,2,3 \ldots\ldots \mathrm{NDISCO} \tag{12}$$

where, $\Delta P_{schedule}$= (Power supply from GENCO in area-a to DISCO in area-b) - (Power flow from GENCO in area-a to DISCO in area-b)

$$\Delta \mathrm{P}_{\mathrm{tie}\ -\mathrm{schedule}} = \sum_{\mathrm{n}=1}^{\mathrm{b}} \sum_{\mathrm{m}=1}^{\mathrm{a}} \mathrm{f}_{\mathrm{nm}} \Delta \mathrm{P}_{\mathrm{Lj}} - \sum_{\mathrm{n}=3}^{\mathrm{a}} \sum_{\mathrm{m}=1}^{\mathrm{b}} \mathrm{f}_{\mathrm{nm}} \Delta \mathrm{P}_{\mathrm{Lj}} \tag{13}$$

The tie-line error at steady state condition is given by:

$$\Delta \mathrm{P}_{\mathrm{tie}-\ \mathrm{error}} = \Delta \mathrm{P}_{\mathrm{tie}-\mathrm{schedule}} - \Delta \mathrm{P}_{\mathrm{tie}-\mathrm{actual}} \tag{14}$$

The tie line error becomes zero when the actual tie-line is equal to the schedule tie-line power flow. The area control mismatch (ACE) signal can be calculated using the tie-line error by using the below mentioned equation.:-

$$\mathrm{E}_1(\mathrm{t}) = \mathrm{ACE}_1 = \mathrm{B}_1 \Delta \mathrm{f}_1 + \Delta \mathrm{P}_{\mathrm{tie1}-2,\mathrm{error}} \tag{15}$$

$$\mathrm{E}_2(\mathrm{t}) = \mathrm{ACE}_2 = \mathrm{B}_2 \Delta \mathrm{f}_2 + \Delta \mathrm{P}_{\mathrm{tie2}-1,\mathrm{error}} \tag{16}$$

$$\text{Where} \quad \Delta \mathrm{P}_{\mathrm{tie1}-2\mathrm{error}} = \alpha_{12} \Delta \mathrm{P}_{\mathrm{tie1}-2\mathrm{error}} \text{ where } (\alpha_{12} = -1) \tag{17}$$

3. Application of Cascade fractional-order hybrid controller (CC-FO hybrid Controller)

In this survey, the LFC of a three-area interconnected network with integrated WPS has been proposed and implemented using a cascade fractional-order hybrid controller (CC-FO hybrid Controller). Create the capacity to reject disturbances while maintaining set-point tracking performance in a multi-loop control system. Over single-loop controllers, cascade controllers have additional advantages in terms of usage are given in [24]. The main objectives of the cascade control scheme in multi-loop systems are shown in Fig. 3

The plant uses an inner-loop (or slave) controller to swiftly mitigate disturbances before they affect other components. Utilizing additional inner-loop limits reduces the effect of changes in internal process parameters (caused by set-point changes, disturbances, etc.) on the operation of the control system.

In the suggested control scheme, 3DOF-PID and FOTID controllers are used as master and slave controllers, respectively. The quantity of closed-loop transfer functions (T.F.) that a control system can use to handle any form of disturbance. The use of 3DOF controllers helps to-

(a) Improve the control system's closed-loop stability.

(b) lessen the impact of disruption and

(c) tracking the set-points and directing the dynamic reaction.

In Fig. 4 depict the symmetric circuit diagram of the suggested 3DOF controller. In Fig. 4 where R(s), D(s), and Y(s) are the predetermined set input, interruption, and calculated system output, respectively; $G_C(s)$ is 1DOF-controller; GRC(s) is the pre-filter controller; $G_{FF}(s)$ is the feed-forward controller; $G_P(s)$ is the process/plant Fig. 3 represent the basic structure of 3DOF-PID controller.

The closed-loop results of the 3DOF controller is acquired as follows:-

In Fig. 3, $G_C(s)$ involves PID-controller with proportional, integral, and derivative gains k_p, k_i, and k_d, respectively, and derivative filter coefficient N, GRC(s) has proportional and derivative set-point weights PW and DW, respectively; $G_{FF}(s)$ has feed-forward gain $k_{ff}(s)$. A newer version of a linear PID controller is the FOTID controller, which serves as the master controller in CC-FO hybrid structures. The FOTID controller has a identical layout to the PID controller, with the exception that non-integer (or fractional) gain is used in place of proportional gain, as shown in Fig. 4. The PID controller model is improved by the inclusion of the non-integer term, which also makes systems more resistant to parameter change.

4. Algorithm

4.1 Particle swarm optimization algorithm

Based on the social behaviour of various animals like flight of birds searching for food and also the swarm movement of the fish, the best option is a random population of variables that are made to migrate in search of food, according to the particle swarm optimization method. The assumed variables or particles moves within the search space with a certain speed. These particles is able to keep track of the previous best position by using a memory. The steps of the algorithm is mentioned below:

1) Initial generation of the particles are determined in a random manner.
2) The present state generation is evaluated using the fitness function.
3) Local best position is stored.
4) Global best position is stored.
5) Position of the particle and its corresponding velocity is updated.
6) If condition = true, process ended.
7) Repeat step 3.

Firstly, memories of each particle is initialized as the best position using their current position. The fitness values of every particle's current position are then compared to their ideal positions. This procedure determines the next best position of the particle denoted by Pos_1 followed by the determination of the Global Best Position denoted by $GPos_1$. In the further steps the values of the next velocity of the particle is calculated using the present velocity values with the value of the distance from the $GPos_1$ and the local ideal place. Next, the modified place of the particle in the search space is pre-planned using value of the velocity calculated earlier this step. Mathematically the velocity and position of each particle is given as follows:

$$V_i^{T+1} = M\,V_i^T + K_1\,N_1(X_{besti}^T - P_i^T) + K_2\,N_2(X_{Gbest}^T - P_i^T) \tag{18}$$

$$P_i^{T+1} = P_i^T + V_i^{T+1} \tag{19}$$

where V_i^T denotes the past velocity of the particle i; P_i^T denotes the position of the ith particle; and X_{besti}^T and X_{Gbest}^T represents, respectively, the particle's local and global best positions. K_1, K_2 and N_1,N_2 denotes the learning coefficients and the random number generated between [0,1], M is the weight coefficient.V_i^{T+1} and P_i^{T+1} denotes the newly modified velocity and particular place of the particle i respectively.

4.2 Whale optimization algorithm

The WOA is the algorithm that the authors of this paper suggest. The widely utilised whale optimization technique was created by Mirjalili and Louise in 2016 and is typically used to tackle global optimization issues more accurately. The competitiveness of this algorithm with similar methods is shown by carrying out its numerical efficiency evaluation. This algorithm's design is based on how humpback whales hunt. The process include hunting on small fish by formation of bubbles and circles on the water surface near its prey, which is termed as bubble net hunting method. There are two types of movement to acquire this namely "upward spiral" and "double loops". In the first type of movement the whale start creating bubbles in a ascending spiral fashion around its prey by going approximately 12m deep into the water and then coming back to the surface after completion. The latter type of movement is achieved through three distinct steps which includes the coral ring, tail tapping, and the catching ring. Further details of the movements is explained in the following paragraphs. The algorithm has three phases to mimic this behaviour:-

i) Identification
ii) Exploitation phase.
iii) Exploration phase.

4.2.1 Identification Phase

The identification phase involves identifying the position of the prey (NOTE: optimal position is unknown) within the search space and encircling it. The other solutions will attempt to update their position with regard to the leading solution during this phase, which is considered the target prey for the leadership solution. The

mathematical equations are given below :

$$\vec{X} = \vec{Y}\,\vec{P} * (t) - \vec{P}(t) \tag{20}$$

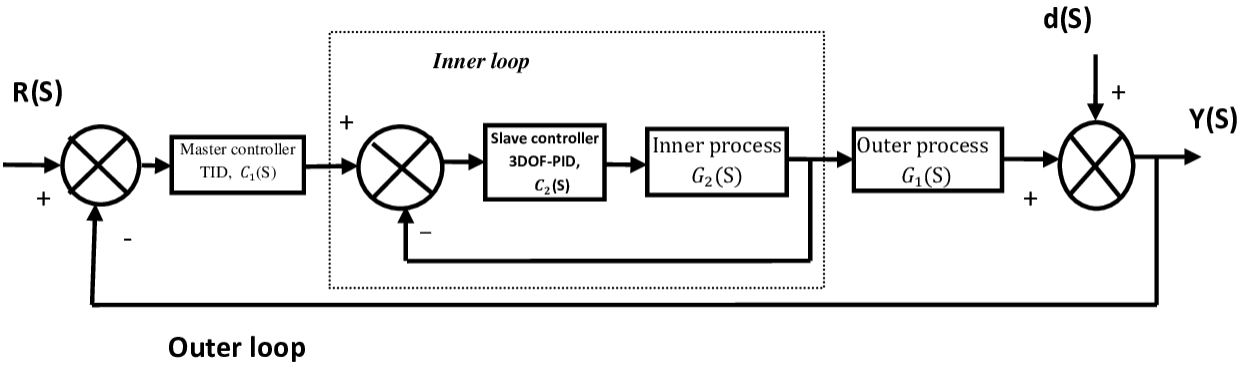

Figure 4: Block structure of cascade controller system

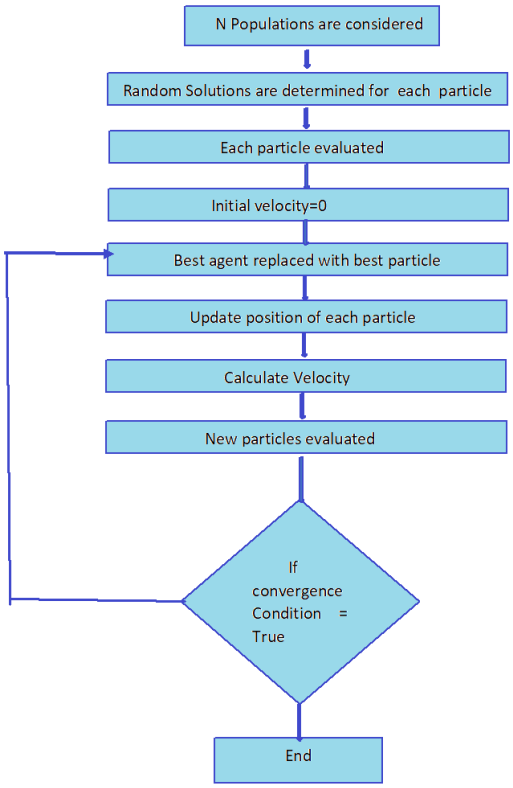

Figure 5: Flowchart of the PSO algorithm

$$\vec{P}(t+1) = \vec{P} * (t) - \vec{Z}\vec{X} \tag{21}$$

given t represent the current iteration$\vec{z}$ also $\vec{Y}$ is the vectors coefficient $\vec{P}$ denotes as a vector location and $\vec{P} * (t)$ denotes the updated location vector, *i.e.*, position given better result detected earlier,which was updated after each iteration.
$\vec{Z}$ and $\vec{Y}$ can be mathematically formulated as shown below:

$$\vec{Z} = 2\vec{z}\vec{v} - \vec{z} \tag{22}$$

$$\vec{Y} = 2\vec{v} \tag{23}$$

Here,$\vec{v}$ denotes the random vector belonging to the range [0,1];$\vec{z}$ is reduced at point 2 to 0 during the survey and taking advantages from survey.

4.2.2 Exploitation phase

In research survey involve the bubble net attacking method. Two mathematical models have been proposed to mimic the bubble-net attacking mechanism of the humpback whale, namely:

i) Shrinking encircling mechanism: The value of the vector $\vec{a}$ is linearly reduced in this manner. The fluctuation on the range of the coefficient vector $\vec{\alpha}$ is between (-$\vec{\alpha}$,$\vec{\alpha}$) depending on vector $\vec{a}$ and random vector $\vec{r}$. The $\vec{a}$ is decreased to 0 which was initially 2.

ii) Spiral updating position: This process involves first calculating the distance between the whale and the prey, after which the whale encircles the prey in a spiralling logarithmic motion. It is assumed that the whale selects the mechanisms with a equal probability of 50 percent. Mathematically,

$$\vec{X}(t+1) = \vec{P}'\, e^{an} \cos(2\pi n) + \vec{X}_1(t) \tag{24}$$

$\vec{P}$ can be mathematically written as:

$$\vec{P} = \vec{X}_1(t) - \vec{X}(t) \tag{25}$$

This $\vec{P}$ denotes the distance between the whale in the ith iteration and the prey; constant a represents the shape of the spiral logarithmic ; n is a arbitrary number between 1 and -1.
Mathematical formulation of the entire process is depicted as under:

$$\vec{X}(t+1) = \{\vec{X}_1(t) - \vec{Z}\vec{X}, p < 0.5 \quad (26)$$

$$\vec{X}(t+1) = \{\vec{X}_1(t) - \vec{Z}\vec{X}, p < 0.5 \quad (27)$$

Apart from using this method the whale also hunts in a random manner. The process is thus as Exploration, which is explained the following paragraph.

4.2.3 Exploration Phase

In the exploration phase the solution of the algorithm is forced to differ from the exact solution and the algorithm randomly explores the search space, by using a random value of the alpha vector greater than +1 or less than -1 and randomly selects the reference solution. The mathematical model is depicted below:

$$\vec{Z} = \vec{X}\,\vec{P}_{rand} - \vec{P} \quad (28)$$

$$\vec{P}(t+1) = \vec{P}_{rand} - \vec{Z}\vec{X} \quad (29)$$

where, $X\vec{rand}$ = position vector of the solution randomly chosen from the current population.

4.3 Hybrid whale optimization algorithm or WOA-PSO algorithm

To compensate the disadvantages of one algorithm while keeping in mind the advantages of the other algorithm, a hybrid version of the algorithm is proposed which is known as hybrid whale optimization algorithm by combining the above mentioned two algorithm namely, whale optimization and particle swarm algorithm. The research step of the suggested approach can make use of numerous test cases. The chosen final solution is the one that performs the best. The proposed algorithm provides better computational speed and faster convergence.

$$V_i^{T+1} = M\,V_i^T + K_1\,N_1(X_{besti}^T - P_i^T) + K_2\,N_2(X_{Gbest}^T - P_i^T) \quad (30)$$

5. Simulation Results and Discussion

The suggested algorithm's viability and efficacy are supported by three areas: thermal with solar, electric vehicle, and wind systems in Fig. 2. On a computer, the entire process was carried out and simulated using MATLAB code. In this study, the crossover operator, represented by, is used to analyse the parameters. 50 people are assumed to be in the population. To achieve better convergence before the last step, a total of 100 iterations were performed. The next paragraphs go into further detail on the two test system:

5.1 (To check the efficacy of HWOT algorithm)

The use of simplified models of various producing units, the LFC of the provided format are in researched. Dynamic system responses may be seen after a load disturbance of around 10%, and then frequency deviation in the specified arena can be seen after that. The effectiveness of the HWOT-tuned PID controller utilised in this article is demonstrated by comparing its dynamic response values to those of other algorithm of a similar type, notably the PSO, WOA and harmony search algorithm (HWOT). The Table 1 contains the suggested optimization. When compared to other algorithm, the HWOT tuned PID controller exhibits a faster rate of improvement in its dynamic responses. Convergence nature of different algorithms are shown in fig. 8(a).

From Table 1, it is observed that 'Δf_1' and 'Δf_2' are improved from that suggested HWOT optimized PID controllers. When compared to the PSO,WOA and WHO optimize by PID controller, the suggested HWOT optimized PID improves ISE, in particular (OBJ), by 95.86%, 92.72% and 60.16% respectively. The efficacy of proposed HWOT algorithm can be investigated by optimizing PID controller, rates of improvement in the dynamic response of "Δf_1" (OS, US & ST) are found to be 9.54 %, 9.7 % and 12.85%; 44.86 %, 33.31% and 24.58 %;31.94%, 48.07% and 3.41% respectively. The efficacy of others algorithms can be investigated by optimizing PID controller through some other techniques such as PSO, WOA and WHO algorithm.

5.2 (To check the efficacy of CCFOHC controller over other controller):-

Case 1: Unilateral Transaction: A three area thermal with solar(PV), wind and electric vehicle(EV) is considered under deregulated environment to design the proposed CCFOHC controller. Unilateral transaction demands every GENCOs to participate equally. The participation factor for different GENCOs are thus listed below: $pf_{11} = 0.5$; $pf_{12} = 1 - 0.5 = 0.5$; $pf_{21} = 0.5$; $pf_{22} = 0.5$. $pf_{31} = 0.5$; $pf_{32} = 0.5$. Consider the change in load in area 1 to be about 0.1pu(MW). For unilateral transaction load disturbance will be seen only in $DISCO_1$ and $DISCO_2$ and in this case the $DISCO_3$ & $DISCO_4$ do not have any demand from the GENCOs. In order to sustain the frequency of steady state the load demand should compulsorily be able to meet the contracted demand between the DISCOs and GENCOs. The amount of load needed by the DISCOs is represented by the coefficient of the participation factor of various GENCOs.

Let demanded load for the suggested DISCOs, *i.e.*, $DISCO_1$ and $DISCO_2$ be ΔP_{L1} and ΔP_{L2}, respectively, and let $\Delta P_{L1} = 0.1\ p.u$ (M.w). Considering these values the cor-

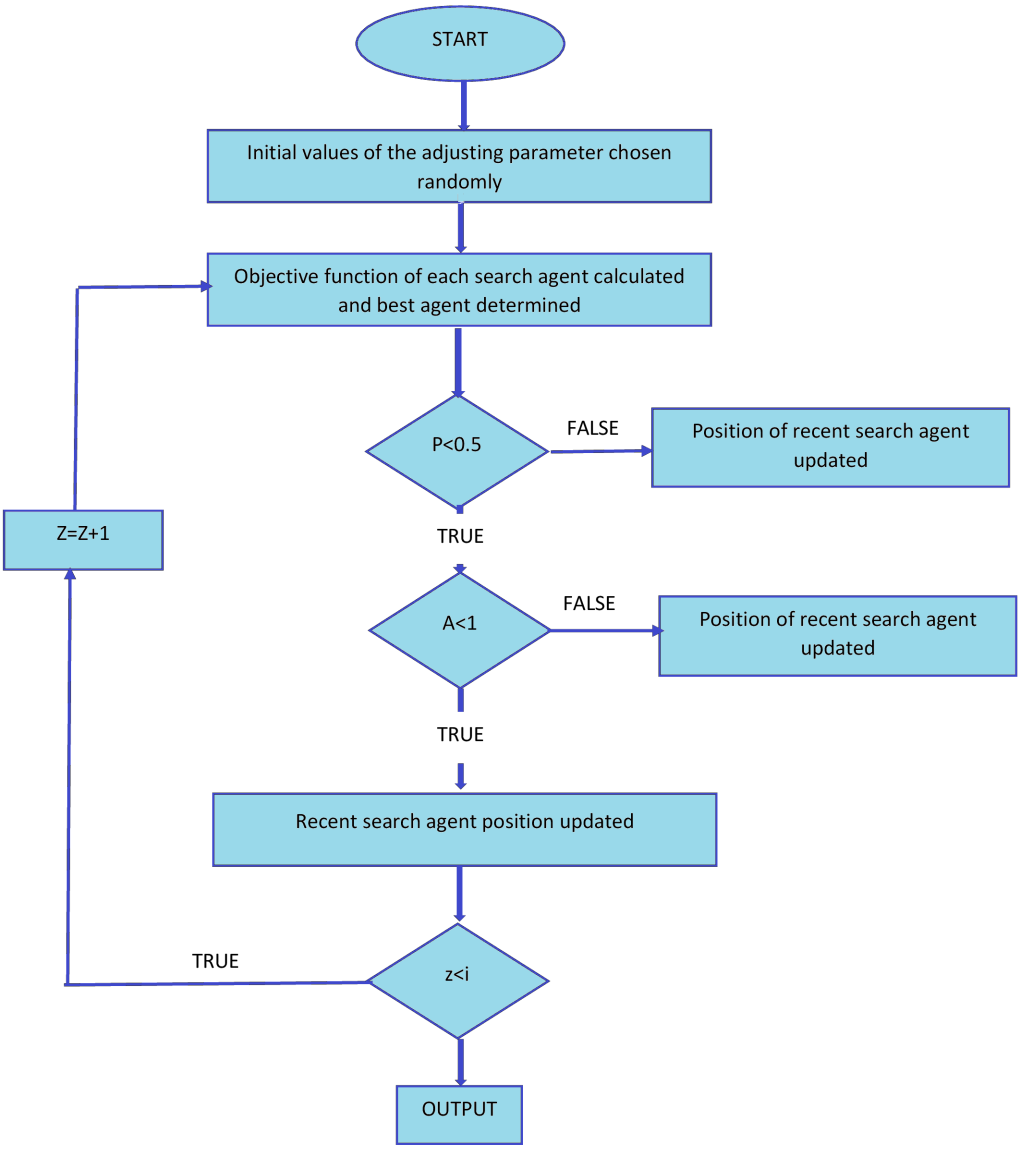

Figure 6: Flowchart of HWOA algorithm

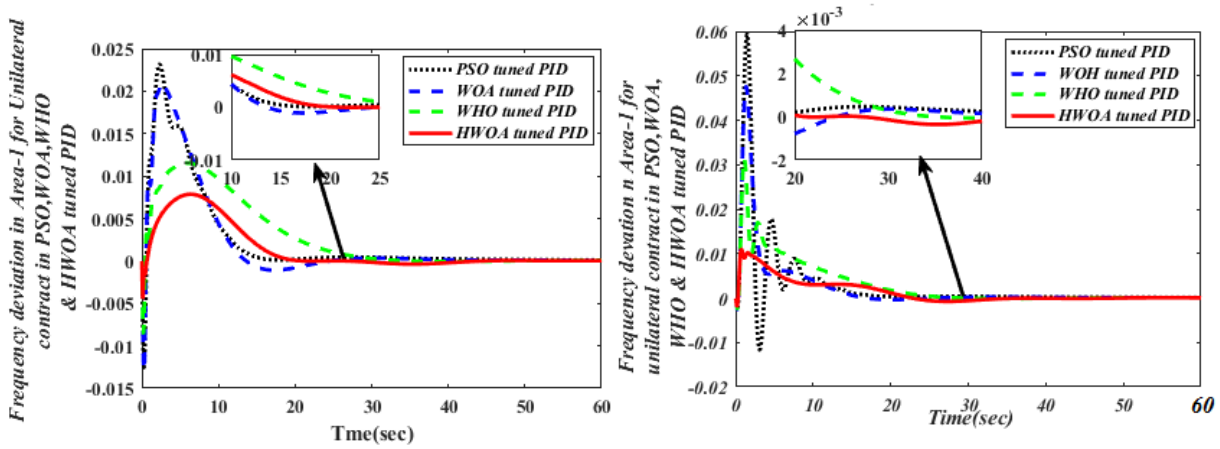

Figure 7: (a) Area-1 frequency variation for Unilateral contract in PSO, WOA,WHO & HWOA tuned PID (b) Area-2 frequency variation for Unilateral contract in PSO, WOA,WHO & HWOA tuned PID

Table 1: PID controller gain values for a two-area system

PID controller	K_{p1}	K_{i1}	K_{d1}	K_{p2}	K_{i2}	K_{d2}	K_{p3}	K_{i3}	K_{d3}	$(OBJ \times 10^{-5})$	Δf_1			Δf_2		
											$OS \times 10^{-6}$	$US \times 10^{-4}$	SS	$OS \times 10^{-6}$	$US \times 10^{-4}$	SS
PSO [14]	0.4817	0.2647	0.7899	0.0489	0.5750	0.0104	0.8174	0.5756	0.7016	1.194	0.00786	-0.004425	45.9	0.01085	-0.0007411	36.41
WOA [28]	0.548	0.2974	0.8155	0.0989	0.7761	0.02045	0.9547	0.5857	0.9474	0.679	0.01155	-0.008522	39.99	0.0313	0	30.75
WHO[1]	0.5321	0.3021	0.7752	0.0882	0.7028	0.7025	0.03021	0.9021	0.5025	0.124	0.02095	-0.01278	30.16	0.04698	-0.0002004	29.59
HWOT	0.11725	0.23107	0.74753	0.29515	0.8642	0.82254	0.71175	0.13958	0.938	0.0494	0.02316	-0.01154	29.13	0.0591	-0.01152	25.33

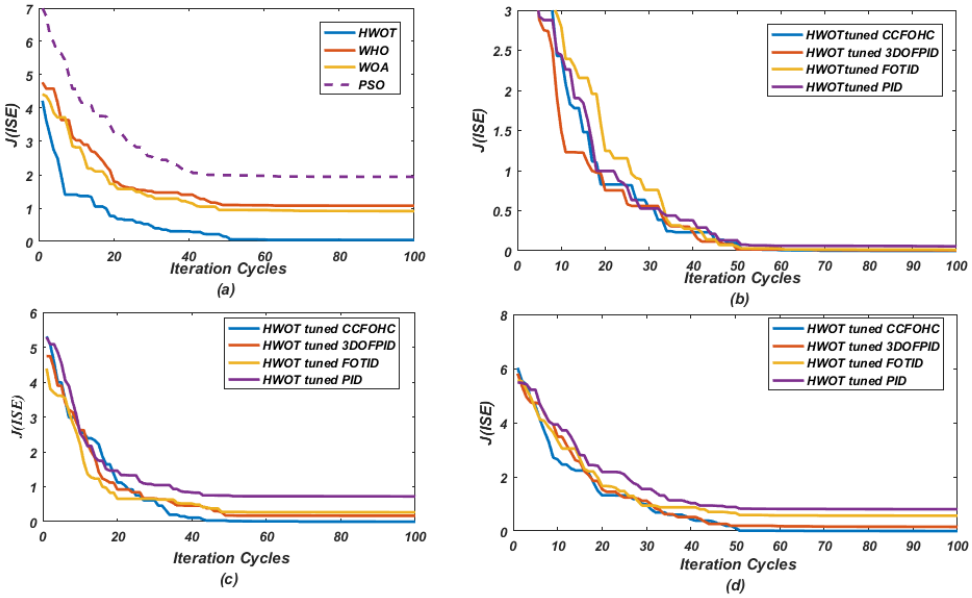

Figure 8: (a) Convergence plotting for different algorithm (b) Case-1 Convergence plotting for HWOT tuned with different controller in unilateral contract (c) Case-2 Convergence plotting for HWOT tuned with different controller in bilateral contract (d) Case-3 Convergence plotting for HWOT tuned with different controller in contract violation .

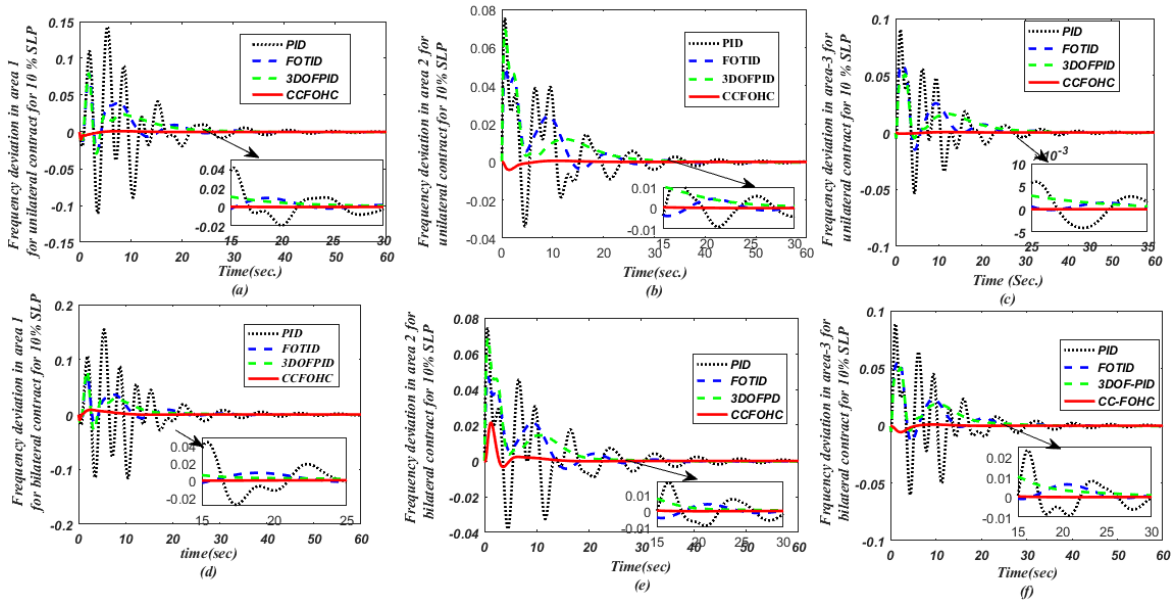

Figure 9: (a) Frequency variation for area-1 in Hz for a disturbance of 10% step load under a unilateral scenario (b) Frequency variation for area-2 in Hz for a disturbance of 10% step load under a unilateral scenario (c) Frequency variation for area-3 in Hz with a step load disturbance of 10% under a unilateral scenario (d) Area-1 frequency deviation in Hz for a step load disturbance of 10% in a bilateral scenario (e) Area-2 frequency deviation in Hz for a step load disturbance of 10% in a bilateral scenario (f) Area-3 frequency deviation in Hz for a step load disturbance of 10% in a bilateral scenario

Table 2: Gain values of FOTID optimised using HWOT algorithm

Type of controllers	Optimized parameters	Unilateral Contract (DPM)				Bilateral Contract (DPM_1)				Contract Violation (DPM_1)			
		CCFOHC	3DOFPID	FOTID	PID	CCFOHC	3DOFPID	FOTID	PID	CCFOHC	3DOFPID	FOTID	PID
FOTID	K_P	0.5728	0.987	0.7723	0.2968	0.6852	0.895	0.2568	0.9498	0.2297	0.987	0.1761	0.3594
	K_I	0.6218	0.427	0.5794	0.5398	0.1128	0.415	0.5328	0.2894	0.6091	0.427	0.1827	0.2954
	K_D	0.1019	0.9958	0.602		0.2215	0.8450	0.7720		0.1005	0.9958	0.26402	
	K_{PW}	0.5021	0.684	0.1546	0.3853	0.0521	0.6592	0.3789	0.1398	0.7425	0.68411	0.01456	0.1358
	K_{DW}	0.835	0.631	-	-	0.7792	0.895	-	-	0.2297	0.987	-	-
	n	3	-	3	-	3	-	3	-	3	-	3	-
	N	0.5021	0.684	0.1546	0.3853	0.0521	0.6592	0.3789	0.1398	0.7425	0.68411	0.01456	0.1358

Table 3: Undershoot (US), overshoot (OS) and settling time (ST) using HWOT tuned 3DOFPID & for step load.

Function	parameters	Unilateral Contract (DPM)				Bilateral Contract (DPM_1)				Contract Violation (DPM_1)			
		CCFOHC	3DOFPID	FOTID	PID	CCFOHC	3DOFPID	FOTID	PID	CCFOHC	3DOFPID	FOTID	PID
Δf_1	OS	0.0008466	0.07565	0.07867	0.142	0.008504	0.05103	0.05858	0.08953	0.00837	0.07722	0.07241	0.1562
	US	-0.01011	-0.02472	-0.02705	-0.1111	-0.001047	-0.00447	-0.01464	-0.05279	-0.0009665	-0.03382	-0.01689	-0.1142
	ST	5.27	33.15	38.44	57.05	8.84	39.1	33.25	56.49	16.79	28.74	29.86	56.98
Δf_2	OS	0.0006	0.06894	0.04899	0.07504	0.02135	0.06823	0.06864	0.0741	0.02131	0.06981	0.04908	0.07376
	US	-0.004149	0	-0.003723	-0.03294	-0.00332	0	0	-0.03676	-0.003349	0	-0.004358	-0.03796
	ST	10.12	37.57	41.31	59.12	18.23	29.91	31.22	58.84	23.29	31.25	41.62	59.19
Δf_3	OS	0.0003146	0.05102	0.05883	0.09022	0.00104	0.05029	0.05492	0.08812	0.00104	0.0499	0.05707	0.08869
	US	-0.00105	-0.004598	-0.01495	-0.0532	-0.005611	-0.003919	-0.01393	-0.06041	-0.00561	-0.004484	-0.01155	-0.05841
	ST	10.81	35.72	39.79	53.18	10.67	32.08	35.06	54.52	16.07	32.36	36.53	57.18
OBJ		2.362×10^{-4}	0.0057	0.0134	0.05612	7.1619×10^{-4}	0.1680	0.2684	0.724	0.0015	0.1551	0.5687	0.8659
Time of simulation (s)		13.04	17.25	12.25	14.61	13.25	12.25	14.45	12.25	14.25	12.25	13.25	15.21

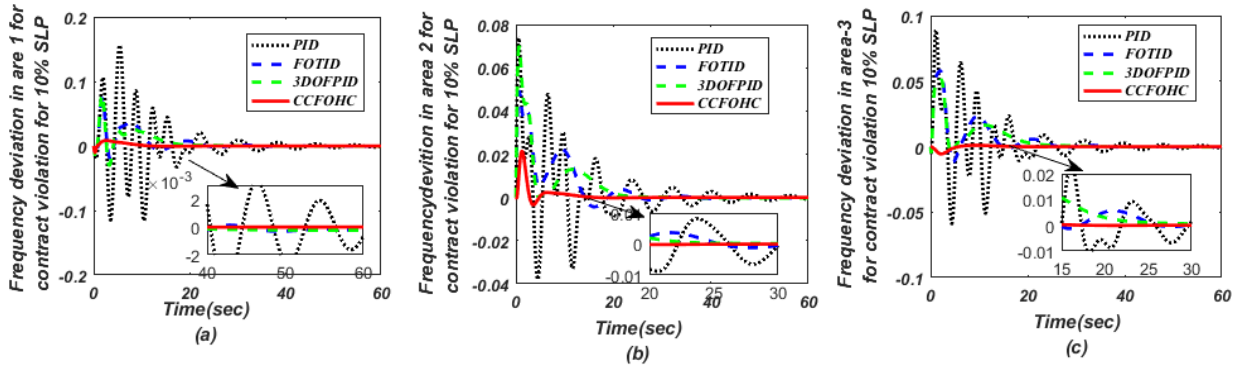

Figure 10: (a) Area-1 frequency variation in Hz for a disruption of 10% step load under a contract breach condition (b) Area-2 Frequency variation in Hz for a disruption of 10% step load under the condition of contract violation (c) Area-3 frequency variation in Hz under a contract breach circumstance with a step load disturbance of 10%.

responding DPM is given below:

$$\text{DPM} = \begin{bmatrix} 0.5 & 0.5 & 0 & 0 & 0 & 0 \\ 0.5 & 0.5 & 0 & 0 & 0 & 0 \\ 0 & 0 & 0 & 0 & 0 & 0 \\ 0 & 0 & 0 & 0 & 0 & 0 \\ 0 & 0 & 0 & 0 & 0 & 0 \\ 0 & 0 & 0 & 0 & 0 & 0 \\ 0 & 0 & 0 & 0 & 0 & 0 \\ 0 & 0 & 0 & 0 & 0 & 0 \end{bmatrix} \tag{31}$$

Now, to maintain the steady state condition the amount of power generated by the GENCOs must be capable of meeting the load demand of each DISCO. The matrix for the desired generation is illustrated below:

$$\begin{bmatrix} \Delta P_{g1ss} \\ \Delta P_{g2ss} \\ \Delta P_{g3ss} \\ \Delta P_{g4ss} \\ \Delta P_{g5ss} \\ \Delta P_{g6ss} \end{bmatrix} = \begin{bmatrix} 0.5 & 0.5 & 0 & 0 & 0 & 0 \\ 0.5 & 0.5 & 0 & 0 & 0 & 0 \\ 0 & 0 & 0 & 0 & 0 & 0 \\ 0 & 0 & 0 & 0 & 0 & 0 \\ 0 & 0 & 0 & 0 & 0 & 0 \\ 0 & 0 & 0 & 0 & 0 & 0 \end{bmatrix} \begin{bmatrix} 0.1 \\ 0.1 \\ 0.0 \\ 0.0 \\ 0.0 \\ 0.0 \end{bmatrix} \tag{32}$$

At first the proposed algorithm, namely, hybrid whale optimization algorithm (HWOT) is used to tune controllers such as Cascade fractional order hybrid controller (CCFOHC), Tilt integral derivative controller(TID), Three degree freedom PID controller(3DOF-PID) & PID controller. It is observed that for the Cascade fractional order tilt-integral-derivative Controller stability is obtained at a faster rate within less time as compared to that of other controllers. The values of the parameters and the corresponding values of overshoot, undershoot and settling time for various controllers are illustrated in Table 2 and Table 3 respectively. Referring to Table 2, it can further be concluded that the accomplished results of all the controller tuned by the proposed algorithm are below the maximum operating limit. Similarly, referring to Table 3 it can be inferred that the best results are obtained using HWOT tuned CCFOHC controllers than using any other type of controllers. The dynamic responses are depicted in the 9(a)-9(c). These Fig. 9 illustrates the frequency deviation and the corresponding tie-line power errors in both the test systems operated under unilateral mode of transaction.

Initially, the percentage of improvement in overshoot, undershoot and settling time for Δf_1 is observed. The improvement of overshoot, undershoot and settling time using CCFOHC controller are 98.880%, 59.101% and 99.12% as compared to those obtained by 3DOF-PID. Moreover, the percentage improvement in objective function using proposed controller is 95.57% as compared to 3DOF-PID controller. Furthermore, to judge the impacts of newly proposed CCFOHC controller and to suppress the oscillations, CCFOHC is applied to the same system. Convergence graph of different controller with proposed controller (CCFOHC) are shown in fig. 8(b) for unilateral case.

From Table 3, it is concluded that the dynamic responses of Δf_1, Δf_2 & Δf_3 are significantly improved using the proposed HWOT optimized CCFOHC controller. The objective function (ISE) is improved by 95.38%, 98.05% & 99.53% respectively, with the proposed HWOT optimized CCFOHC as compared to 3DOF-PID, FOTID and PID controller. From the dynamic, it is concluded that HWOT optimized CCFOHC controller has best dynamic responses than any other optimized controllers.

Case 2 : Bilateral Transactions : To verify the technique and to judge the efficiency of the technique the above mentioned system is now under bilateral mode of transaction. In this mode of transaction the DISCOs are allowed to make contract with the GENCOs of its own area as well as GENCOs of other areas. DISCOs making contract with GENCOs of other areas will result in different values of cpfs of the DPM matrix. Thus, two different matrices namely (DPM_1 and DPM_2) have been considered here.

The first matrix DPM_1 can be given mathematically as :

$$DPM_1 = \begin{bmatrix} 0.15 & 0.35 & 0.15 & 0.25 & 0.1 & 0.15 \\ 0.1 & 0.10 & 0.2 & 0.15 & 0.15 & 0.25 \\ 0.25 & 0.15 & 0.1 & 0.15 & 0.15 & 0.3 \\ 0.2 & 0.2 & 0.15 & 0.1 & 0.2 & 0.1 \\ 0.1 & 0.1 & 0.2 & 0.15 & 0.2 & 0.1 \\ 0.2 & 0.1 & 0.2 & 0.15 & 0.2 & 0.1 \end{bmatrix} \quad (33)$$

$P_{g1ss} = f_{11} \times \Delta P_{L1} + f_{12} \times \Delta P_{L2+} + f_{13} \times \Delta P_{L3}$ $+ f_{14} \times \Delta P_{L4} + f_{15} \times \Delta P_{L5} + f_{16} \times \Delta P_{L6} = 0.15 \times 0.1 + 0.35 \times 0.1 + 0.15 \times 0.1 + 0.25 \times 0.1 + 0.15 \times 0.1 + 0.15 \times 0.1$ $= 0.12 M.w$(p.u).

Likewise, the matrix 2 DPM_2 can be written as under:

$$\left.\begin{array}{c} \Delta \mathrm{P_{g2ss}} = 0.095\mathrm{Pu\ Mw}; \\ \Delta \mathrm{P_{g3ss}} = 0.11\mathrm{Pu\ Mw}; \\ \Delta \mathrm{P_{g4ss}} = 0.095\mathrm{Pu\ Mw}; \\ \Delta \mathrm{P_{g5ss}} = 0.085\mathrm{Pu\ Mw}; \\ \Delta \mathrm{P_{g6ss}} = 0.095\mathrm{Pu\ Mw}; \end{array}\right\} \quad (34)$$

$$DPM_2 = \begin{bmatrix} 0.2 & 0.1 & 0.15 & 0.3 & 0.25 & 0.2 \\ 0.15 & 0.25 & 0.1 & 0.2 & 0.15 & 0.35 \\ 0.35 & 0.15 & 0.25 & 0.15 & 0.1 & 0.15 \\ 0.1 & 0.2 & 0.15 & 0.15 & 0.25 & 0.2 \\ 0.1 & 0.15 & 0.1 & 0.1 & 0.15 & 0.1 \\ 0.1 & 0.15 & 0.25 & 0.1 & 0.1 & 0.1 \end{bmatrix} \quad (35)$$

Dynamic responses of this matrix is now compared with those obtained using the CCFOHC controller tuned using hybrid whale optimization algorithm. In Table 2, the matching optimal values are displayed. It is evident from Table 3 that the suggested controller, the CCFOHC controller, was optimised using the HWOT algorithm provides a better and more superior range of values of undershoot, overshoot, settling time and the fitness coefficients. Now, the steady state values of powers generated by each GENCO is presented below.

$$\left.\begin{array}{c} \Delta\mathrm{Pg1ss}{=}0.3\ \mathrm{pu\ (MW)} \\ \Delta\mathrm{Pg2ss}{=}0.12\mathrm{pu\ (MW)} \\ \Delta\mathrm{Pg3ss}{=}0.115\mathrm{pu\ (MW)} \\ \Delta\mathrm{Pg4ss}{=}0.105\mathrm{pu\ (MW)} \\ \Delta\mathrm{Pg5ss}{=}0.07\mathrm{pu\ (MW)} \\ \Delta\mathrm{Pg6ss}{=}0.08\mathrm{pu\ (MW)} \end{array}\right\} \quad (36)$$

The results achieved are now compared with those obtained for the different controllers. This helps us in analyzing the matrix DPM_2. Table 3 gives a reference regarding the frequency settling time for three different area. It is observed from Fig. 9(d)-8(f) that the coordinated controllers Fig. 9 reduce the peak overshoot, undershoot, and settling time of the system output. As a result, we concluded from aforementioned output that the suggested CCFOHC controller, which was optimised using the HWOT technique, exhibits better dynamic responses than various controllers in terms of their undershoot, overshoot, and settling times. Convergence graph of different controller with proposed controller (CCFOHC) are shown in fig. 8(c) for bilateral case.

Case 3: Contract violation: For further analysis the considered system is now put under contract violation condition. In this mode of operation the DISCOs are made to violate the contract norms that is it draws more amount of power than the upper limit of the actual contract. Here, DPM_2 indicates GENCOs. In this particular situation $DISCO_1$ is drawing power 0.1 *p.u.* (MW) more than that demanded in the actual bilateral contract. Here, ΔP_{uc1}=0.1 pu MW and on the other hand ΔP_{uc2}=0.0; ΔP_{uc3} =0.0; ΔP_{uc4}=0.0. Different cases are considered identical to that used in Bilateral transaction. As a result,ΔP_{uc1}+ ΔP_{uc2}=$\Delta P_{uc1,Loc1}$ = 0.1+0.0 = 0.1 pu MW and $\Delta P_{uc1,Loc2}$= ΔP_{uc3}+ΔP_{uc4}= 0.0 *p.u* (M.w). The ACE involvement factor is also the same as in case of Bilateral Transaction which helps to distribute the excessive power drawn effectively among all the GENCOs (belonging to same area). The equations given below determines the steady state value of power generated by individual GENCOs for the matrix DPM_1 :

$$\left.\begin{array}{c} \Delta Pg_{1ss} = 0.165 PuMw; \\ \Delta Pg_{2ss} = 0.115 PuMw; \\ \Delta Pg_{3ss} = 0.13 PuMw; \\ \Delta Pg_{4ss} = 0.055 uMw; \\ \Delta Pg_{5ss} = 0.0285 PuMw; \\ \Delta Pg_{6ss} = 0.125 PuMw; \end{array}\right\} \quad (37)$$

Similarly, the equations given below determines the steady state value of power generated by each GENCOs for the matrix DPM_2.

$$\left.\begin{array}{c} \Delta\mathrm{Pg1ss}{=}0.15\ \mathrm{pu\ (MW)} \\ \Delta\mathrm{Pg2ss}{=}0.16\ \mathrm{pu\ (MW)} \\ \Delta\mathrm{Pg3ss}{=}0.165\ \mathrm{pu\ (MW)} \\ \Delta\mathrm{Pg4ss}{=}0.495\ \mathrm{pu\ (MW)} \\ \Delta\mathrm{Pg3ss}{=}0.105\ \mathrm{pu\ (MW)} \\ \Delta\mathrm{Pg4ss}{=}0.375\ \mathrm{pu\ (MW)} \end{array}\right\} \quad (38)$$

Table 2 lists the various optimal values of the proposed controller tuned using HWOT obtained for the matrices DPM_1 and DPM_2. From Fig. 10(a)-9(c) it is observed that the values of overshoot, undershoot, settling time of frequency variation are Fig. 10 impressively minimized also allowing the search over larger search spaces. This led to the conclusion that the proposed controller(CCFOHC) can be considered superior as compared to other similar controllers. Convergence graph of different controller with proposed controller (CCFOHC) are shown in fig. 8(d) for contract violation case.

6. System robustness evaluation with RLP Load

The test system 2 is now put under RLP load to judge fitness of the system Fig. 11(a) illustrates the profile of continuous load perturbation by varying it by $\pm 0.02 p.u(Mw)$. Now, a comparative survey with various controller combinations for the same test system under the same conditions had been done to demonstrate the effectiveness of the utilised controller. From Fig. 11(b)-10(d) It is evident that Fig. 11 the values of settling time of frequency and the various tie line power variations are decreased to a minimal value when utilising CCFOHC controller. As a result, it is evident from this figure that the developed controller, which was optimised using the hybrid

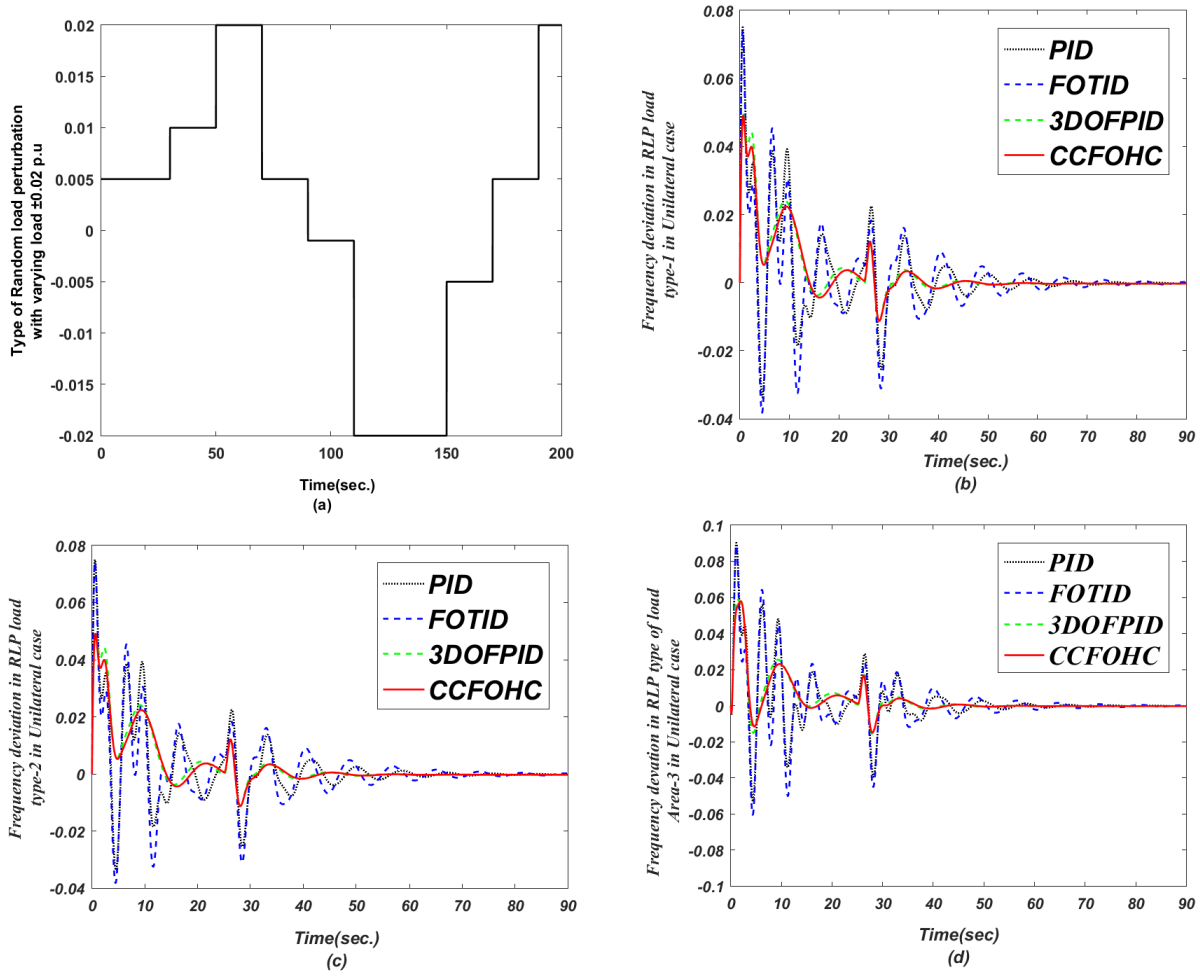

Figure 11: (a) Pattern of the Random Load Perturbation (RLP) with varing load ±0.02 p.u (b) Area-1 frequency variation in RLP load in Unilateral contract (c) Area-2 Frequency variation in RLP load in Bilateral contract (d) Area-3 Frequency deviation in RLP load in contract violation

Table 4: Output Gain of CCFOHC controller with HWOT algorithm for RLP type of load

Optimized parameters	Unilateral Contract (DPM)				Bilateral Contract (DPM_1)				Contract Violation (DPM_1)			
	CCFOHC	3DOFPID	FOTID	PID	CCFOHC	3DOFPID	FOTID	PID	CCFOHC	3DOFPID	FOTID	PID
K_P	0.3917	0.5754	0.9082	0.3345	0.6128	0.2358	0.7254	0.2231	0.3012	0.325	0.254	0.265
K_I	0.4525	0.1020	0.445	0.5528	0.2928	0.6251	0.4325	0.1805	0.2015	0.235	0.526	0.895
K_D	0.758	0.3021	0.8891	0.6958	0.6821	0.1021	0.457	0.0152	0.3524	0.256	0.235	0.458
K_T	0.4657	0.02451	0.7750		0.2292	0.04651	0.7887		0.1541	0.564	0.464	
λ	0.8258	0.6521	-	-	0.18925	0.04428	-	-	0.1157	0.235	-	-
n	3				3				3			
N	0.9128	-	0.7651	-	0.325	-	0.1021	-	0.01128	-	0.0256	-
OBJ	1.257×10^{-4}	0.0287	0.475	4.125×10^{-4}	0.0451	0.452	0.0085	0.0214	0.9214	0.235	0.562	0.248

whale optimization method, is able to control disturbances in a deregulated environment more effectively and to achieve the required goals Table 4.

7. Conclusion

This literature presents a detailed analysis of the area frequency oscillations and the tie-line power error provided that the test systems are considered under uncontrolled condition. The load is varied and effect of these load perturbations are studied with the help of a simplified model of the CC-FOHC tuned with the use of hybrid whale optimised algorithm (HWOT), and the corresponding outputs are compared with the results of different controllers namely 3DOF-PID, FOTID & PID controller. A detailed comparative study of the different used controllers had been provided in this literature assuring better performance by the CCFOTID controller. Various stressful situations and cases are considered like the Unilateral transaction, bilateral transaction, and the contract violation to assure the effectiveness and the efficiency of the implemented hybrid whale optimisation algorithm under deregulation based Automatic Generation Control (AGC).

Thus, the proposed controller can be effectively employed in applications governing the Automatic Generation Control (AGC) to circumvent the possible difficulties and uncertainties faced while replacing conventional energy resources with the non-conventional one in the near future.

8. Appendices

Appendix A. Parameters of the test system's nominal values (PV-Wind-Solar Plant): $B_1, B_2 = 0.425 p.u\ MW/Hz$; $R_1, R_2 = 2.4 Hz/pu$; $T_{G1} = 0.08s$; $T_{T1} = 0.3s$; $T_{r1} = 10s$; $K_{r1} = 0.3s$; $K_{P1} = 120 Hz/puMW$; $K_{WT1} = 1.25$; $T_{TP1,WT1} = 0.65$; $T_{TP2,WT2} = 0.3$; $K_{P2} = 120 Hz\ /pu\ MW$; $T_{TPWA} = 0.67s$; $K_{TPWA} = 0.3$; $T_{P1} = T_{P2} = 20s$; $Ptie12 = 200\ MW$; $a12 = -1$, $RLP = \pm 0.02 p.u(Mw)$ $a = 900$; $b = -18$; $d = 50$; $d = 50$; $T_W = 1sec$

REFERENCES

[1] Soumen Biswas, Provas Kumar Roy, and Kalyan Chatterjee. Facts-based 3dof-pid controller for lfc of renewable power system under deregulation using goa. *IETE Journal of Research*, pages 1–14, 2021.

[2] Dillip Khamari, Rabindra Kumar Sahu, Tulasichandra Sekhar Gorripotu, and Sidhartha Panda. Automatic generation control of power system in deregulated environment using hybrid tlbo and pattern search technique. *Ain Shams Engineering Journal*, 11(3):553–573, 2020.

[3] Sonali Priyadarshani, KR Subhashini, and JK Satapathy. Pathfinder algorithm optimized fractional order tilt-integral-derivative (fotid) controller for automatic generation control of multi-source power system. *Microsystem Technologies*, 27(1):23–35, 2021.

[4] Vikas Soni, Girish Parmar, and Mithilesh Kumar. A hybrid grey wolf optimisation and pattern search algorithm for automatic generation control of multi-area interconnected power systems. *International Journal of Advanced Intelligence Paradigms*, 18(3):265–293, 2021.

[5] Rabindra Kumar Sahu, GT Sekhar, and Sonali Priyadarshani. Differential evolution algorithm tuned tilt integral derivative controller with filter controller for automatic generation control. *Evolutionary Intelligence*, 14(1):5–20, 2021.

[6] Yogendra Arya. A new optimized fuzzy fopi-fopd controller for automatic generation control of electric power systems. *Journal of the Franklin Institute*, 356(11):5611–5629, 2019.

[7] Jyoti Ranjan Nayak, Binod Shaw, and Binod Kumar Sahu. Application of adaptive-sos (asos) algorithm based interval type-2 fuzzy-pid controller with derivative filter for automatic generation control of an interconnected power system. *Engineering Science and Technology, an International Journal*, 21(3):465–485, 2018.

[8] Jyoti Ranjan Nayak, Binod Shaw, and Binod Kumar Sahu. Automatic generation control of small hydro plants integrated multi-area system using fuzzy based symbiotic organism search optimized hybrid piλd fuzzy-piλd controller. *International Transactions on Electrical Energy Systems*, page e12954, 2021.

[9] KS Rajesh, SS Dash, and Ragam Rajagopal. Hybrid improved firefly-pattern search optimized fuzzy aided pid controller for automatic generation control of power systems with multi-type generations. *Swarm and evolutionary computation*, 44:200–211, 2019.

[10] Kumaraswamy Simhadri, BVS Acharyulu, Banaja Mohanty, and K Suneel Goutham. Woa optimized 2dof tidf controller for automatic generation control of hydro-thermal system. In *Intelligent Computing in Control and Communication*, pages 519–527. Springer, 2021.

[11] SS Dhillon, Surabhi Agarwal, Gai-Ge Wang, and JS Lather. Automatic generation control of interconnected power systems using elephant herding optimization. In *Intelligent Computing Techniques for Smart Energy Systems*, pages 9–18. Springer, 2020.

[12] Andrew Xavier Raj Irudayaraj, Noor Izzri Abdul Wahab, Mallapu Gopinath Umamaheswari, Mohd Amran Mohd Radzi, Nasri Bin Sulaiman, Veerapandiyan Veerasamy, SC Prasanna, and Rajeswari Ramachandran. A matignon's theorem based stability analysis of hybrid power system for automatic load frequency control using atom search optimized fopid controller. *IEEE Access*, 8:168751–168772, 2020.

[13] Mokhtar Shouran, Fatih Anayi, Michael Packianather, and Monier Habil. Load frequency control based on the bees algorithm for the great britain power system. *Designs*, 5(3):50, 2021.

[14] Mahendra Kumar and Yogesh V Hote. Robust pidd2 controller design for perturbed load frequency control of an interconnected time-delayed power systems. *IEEE Transactions on Control Systems Technology*, 2020.

[15] Amir Bagheri, Ali Jabbari, and Saleh Mobayen. An intelligent abc-based terminal sliding mode controller for load-frequency control of islanded micro-grids. *Sustainable Cities and Society*, 64:102544, 2021.

[16] Neda Jalali, Hadi Razmi, and Hasan Doagou-Mojarrad. Optimized fuzzy self-tuning pid controller design based on tribe-de optimization algorithm and rule weight adjustment method for load frequency control of interconnected multi-area power systems. *Applied Soft Computing*, 93:106424, 2020.

[17] Mohamed A Sobhy, Almoataz Y Abdelaziz, Hany M Hasanien, and Mohamed Ezzat. Marine predators algorithm for load frequency control of modern interconnected power systems including renewable energy sources and energy storage units. *Ain Shams Engineering Journal*, 2021.

[18] Emre Çelik. Design of new fractional order pi–fractional order pd cascade controller through dragonfly search algorithm for advanced load frequency control of power systems. *Soft Computing*, 25(2):1193–1217, 2021.

[19] Dipayan Guha, Provas K Roy, and Subrata Banerjee. Equilibrium optimizer-tuned cascade fractional-order 3dof-pid controller in load frequency control of power system having renewable energy resource integrated. *International Transactions on Electrical Energy Systems*, 31(1):e12702, 2021.

[20] Dalia Yousri, Thaniaknti Sudhakar Babu, and Ahmed Fathy. Recent methodology based harris hawks optimizer for designing load frequency control incorporated in multi-interconnected renewable energy plants. *Sustainable Energy, Grids and Networks*, 22:100352, 2020.

[21] Sonalika Mishra, Suchismita Patel, Ramesh Chandra Prusty, and Sidhartha Panda. Mvo optimized hybrid fofpid-lqg controller for load frequency control of an ac micro-grid system. *World Journal of Engineering*, 2020.

[22] Bhuvnesh Khokhar, Surender Dahiya, and KP Singh Parmar. A novel fractional order proportional integral derivative plus second-order derivative controller for load frequency control. *International Journal of Sustainable Energy*, 40(3):235–252, 2021.

[23] Rajiv Kumar and VK Sharma. Whale optimization controller for load frequency control of a two-area multi-source deregulated power system. *International Journal of Fuzzy Systems*, 22(1):122–137, 2020.

[24] Farhad Amiri and Alireza Hatami. Nonlinear load frequency control of isolated microgrid using fractional order pid based on hybrid craziness-based particle swarm optimization and pattern search. *Journal of Iranian Association of Electrical and Electronics Engineers*, 17(2):135–148, 2020.

[25] Naladi Ram Babu and Lalit Chandra Saikia. Load frequency control of a multi-area system incorporating dish-stirling solar thermal system and coyote optimized pi minus df controller. In *2020 IEEE International Conference on Power Electronics, Smart Grid and Renewable Energy (PESGRE2020)*, pages 1–6. IEEE, 2020.

[26] Erdinc Sahin. Design of an optimized fractional high order differential feedback controller for load frequency control of a multi-area multi-source power system with nonlinearity. *IEEE Access*, 8:12327–12342, 2020.

[27] Ali Dokht Shakibjoo, Mohammad Moradzadeh, Seyed Zeinolabedin Moussavi, Ardashir Mohammadzadeh, and Lieven Vandevelde. Load frequency control for multi-area power systems: A new type-2 fuzzy approach based on levenberg–marquardt algorithm. *ISA transactions*, 2021.

[28] Nizamuddin Hakimuddin, Ibraheem Nasiruddin, Terlochan Singh Bhatti, and Yogendra Arya. Optimal automatic generation control with hydro, thermal, gas, and wind power plants in 2-area interconnected power system. *Electric Power Components and Systems*, 48(6-7):558–571, 2020.